Tribology Letters (2022) 70:102
https://doi.org/10.1007/s11249-022-01644-w

ORIGINAL PAPER

Mechanochemical Ionization: Differentiating Pressure-, Shear-, and Temperature-Induced Reactions in a Model Phosphate

Sergey V. Sukhomlinov[1,2] · Guido Kickelbick[3] · Martin H. Müser[1]

Received: 19 June 2022 / Accepted: 6 August 2022 / Published online: 26 August 2022

Abstract

Using density-functional theory-based molecular dynamics simulations, we study stress and temperature-induced chemical reactions in bulk systems containing triphosphoric acid and zinc phosphate molecules. The nature of the products depends sensitively on the imposed conditions, e.g., isotropic and even more so shear stress create (zwitter-) ionic products. Free ions also emerge from thermal cycles, but the reactions are endothermic rather than exothermic as for stress-induced transitions and zinc atoms remain four-coordinated. Hydrostatic stresses required for reactions to occur lie well below those typical for tribological micro-contacts of stiff solids and are further reduced by shear. Before zinc atoms change their coordination under stress, proton mobility increases, i.e., hydrogen atoms start to change the oxygen atom they are bonded to within 10 ps time scales. The hydrostatic stress for this to occur is reduced with increasing shear. Our finding suggests that materials for which number, nature, and mobility of ions are stress sensitive cannot have a well-defined position in the triboelectric series, since local contact stresses generally depend on the stiffness of the counter body. Moreover, our simulations do not support the idea that chemical reactions in a tribo-contact are commonly those that would be obtained through heating alone.

✉ Martin H. Müser
martin.mueser@mx.uni-saarland.de

[1] Department of Materials Science and Engineering, Saarland University, 66123 Saarbrücken, Germany

[2] INM - Leibniz Institute for New Materials, 66123 Saarbrücken, Germany

[3] Department of Chemistry, Saarland University, 66123 Saarbrücken, Germany

Graphical Abstract

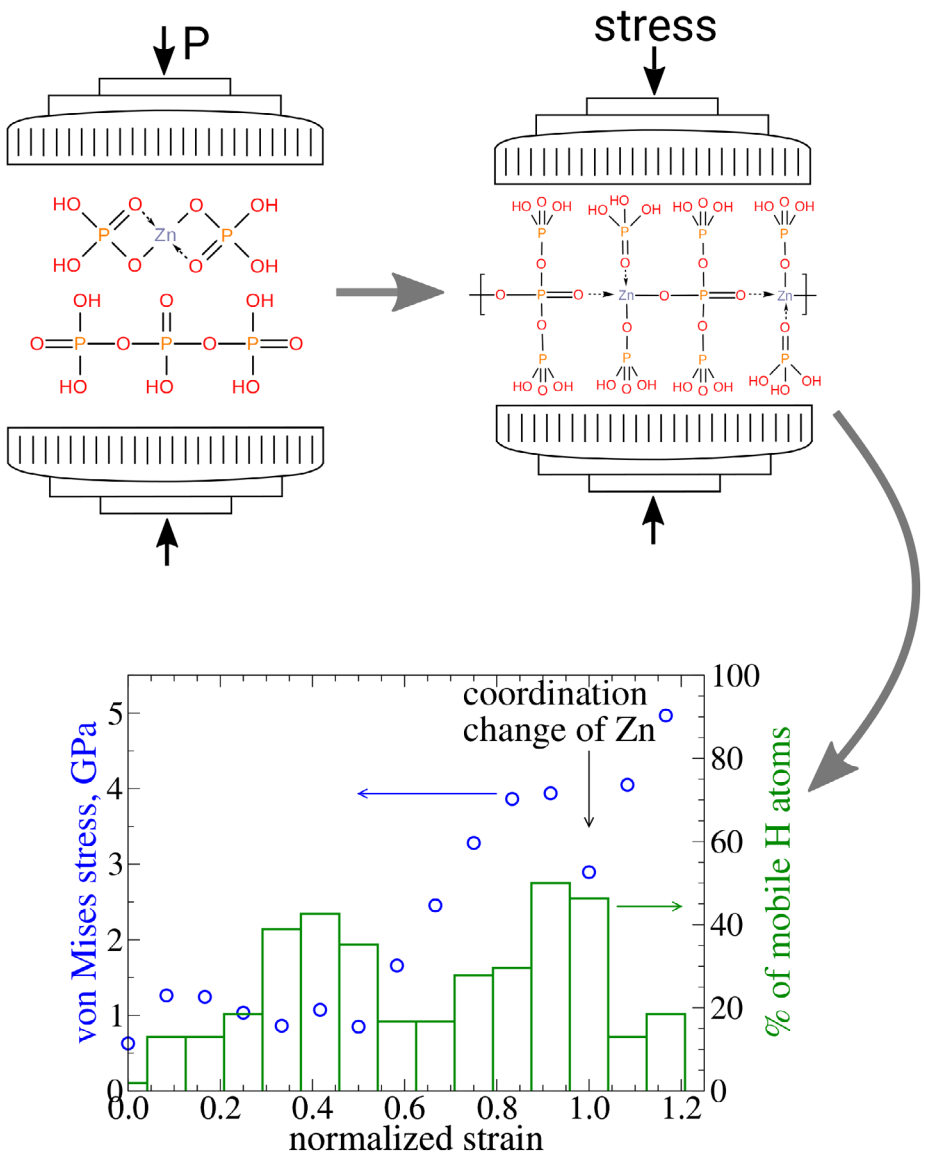

Keywords Tribochemistry · Mechanochemistry · ZDDP · Triboelectricity

1 Introduction

Mechanochemistry is primarily concerned with the interplay of mechanical forces and chemical bonds [1–3]. This includes the analysis of the breaking or unfolding of individual molecules under tensile forces, which is of great scientific interest [1, 4], but also, stress-induced chemical changes in bulk systems under positive hydrostatic stresses, as they occur during ball milling [5] and/or at rubbing interfaces [2, 6], i.e., in tribochemistry. Two questions in mechanochemistry are surprisingly unexplored. First, how does the precise form of the stress tensor affect stress-induced chemical changes? Most works, including influential reviews [1, 2], treat stress as being small or large. However, mathematically speaking, stress is a three-by-three matrix and not simply a scalar. Thus, for certain reactions to be preferentially induced in an originally isotropic system, the three eigenvalues of the stress tensor may have to approach three independent target numbers closely. In other words, generating an optimum condition for a certain reaction to occur could necessitate the simultaneous tuning of

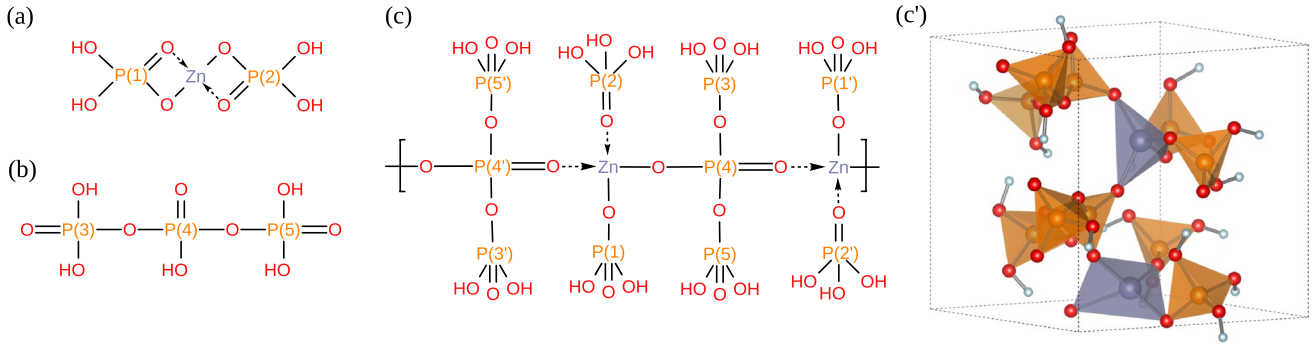

Fig. 1 Lewis structure of the initial molecules, specifically **a** $Zn[PO_4H_2]_2$, **b** $P_3O_{10}H_5$, and **c** Lewis, **c′** three-dimensional structures of the initial structure after compression to $p = 0.5$ GPa. In **c** and **c′**, Zn atoms are drawn in gray, P atoms in orange and O in red. H atoms are drawn in red and in light-blue colors in **c** and **c′**, respectively. The polyhedra color-coding is consistent with its respective central atom. Dashed gray arrows in **a** and **c** indicate ionic bonds and are drawn in the direction from negatively to positively charged atoms. Numbers enumerate phosphor atoms (Color figure online)

shear and hydrostatic stress plus one additional condition, and even more conditions for ordered systems. Second, how do stress and its anisotropy affect the generation of ions and/or their mobility? The answer to this question could be central to correctly explain various observations made on the friction-induced charge transfer between two rubbing, large bandgap insulators, which is one of the earliest studied natural phenomena [7]. In fact, as McCarty and Whitesides [8] discuss very thoroughly, tribo-charging is difficult to explain when not only electrons but also ions appear to be immobile. Thus, a central question to be addressed is how (contact) stress affects number and mobility of ions and not only the electronic band structure.

There is an arsenal of bulk systems for which the precise form of the stress tensor could affect the chemical structure after the external stress is released [9–12], irrespective of whether or not it involves the separation of an interface. We decided to first focus on phosphate-based systems, because their properties appear to be particularly sensitive to external stresses: the formation and functionality of zinc phosphate (ZnPs)-based anti-wear films on rubbing surfaces [13, 14] as well as their patchiness with stiff films occurring on the highly loaded asperities and soft films in the valleys [15] was interpreted as a stress hysteresis [16]. Experiments supported the conjecture that the fast formation of stiff films benefits from hard substrates in that mechanical properties of the substrates were found to be more critical than their stoichiometry [17, 18]. Metal phosphates are also used for many other applications, e.g., as electrolytes in galvanic [19] and fuel cells [20, 21]. The question arises to what extent the conductivity of (metal) phosphates [20–25] can be increased through the application of mechanical stress, given that computer simulations of triphosphoric acid molecules indicated a proton transfer reaction to occur between originally identical and neutral molecules at a hydrostatic pressure of $p \approx 3.5$ GPa, whereby free cations and anions were produced [26]. Related stress-induced processes may explain why the conductivity of a 1:1 mixture of $CsHSO_4$ and CsH_2PO_4 was substantially enhanced through ball milling [24]. The interplay of mechanical stress and phosphate chemistry even appears in organic systems, where mechanically stressing integrin receptors were observed to enhance the tyrosine phosphorylation of cytoskeletally anchored proteins [27]. These few examples are certainly only the tip of the iceberg of cases, in which the stress and its anisotropy affect the chemistry of phosphates and the tip of an entire mountain range if other group-5-element containing (molecular) solids were included.

We have recently studied the response of a bulk system containing triphosphoric acid and zinc phosphate molecules to externally imposed deformations [28]. All compression/decompression cycles lead to exothermic chemical changes, however, the reaction energy, i.e., the energy difference between the fully relaxed initial and final structures, generally turned out largest in magnitude under isotropic deformation and smallest when the deformation was most anisotropic. The bulk modulus of the decompressed structures revealed similar trends. Unfortunately, our previous analysis of the structural or chemical changes in terms of two- and three-body correlation functions did not allow us to rationalize our results. The original motivation of this work was to achieve this with a more detailed analysis of the chemical bonding. We discovered, much to our surprise, that the Lewis structures of the configurations, which were produced while compressing three-dimensional, orthorhombic simulation cells, could be represented in terms of Lewis structures containing a linear ZnP chain plus potentially a protonated phosphoric acid molecule. This feature allowed us to interpret the stress-induced changes in zinc phosphates in rather simple chemical terms and to reveal a process, which might be dubbed stress-induced (zwitter-) ionization. Such a process is likely to have immediate consequences for rubbing or

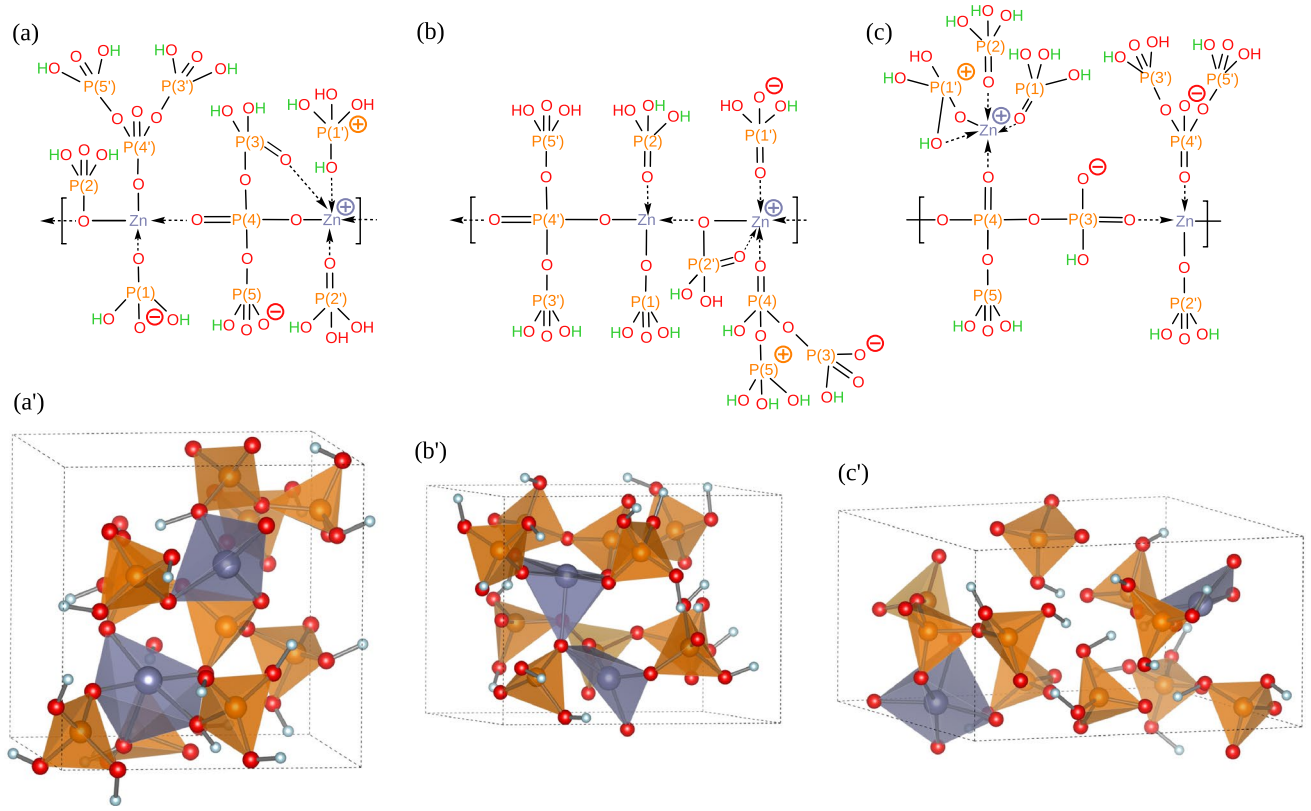

Fig. 2 Lewis (**a**–**c**) and three-dimensional (**a′**–**c′**) structures of the system after decompression from **a** isotropic, **b** uniaxial, and **c** volume-conserving compressions. Dashed arrows indicate ionic bonds. Zinc, phosphorus and oxygen are presented in gray, orange and red colors, respectively. Formal positive charges are always assigned to the phosphor atom in a phosphate group rather than to hydrogen atoms. Two colors were used for hydrogen atoms when drawing Lewis structures: red for those that are bonded to the same oxygen atom before and after the compression and green otherwise (Color figure online)

contact-induced static charge, also known as triboelectricity. While we analyze to a large extent the structures produced during our previous study, we added additional calculations to increase statistics, to better analyze decomposition products, and to study the response of the studied system to heating and cooling.

2 Model and Methods

2.1 Simulation Details

Density-functional theory [29, 30] simulations are done using the same CP2K open-source package [31] and similar methodology as our precedent paper [28], including the Perdew–Burke–Ernzerhof exchange–correlation functional [32] with Grimme empirical corrections to the dispersion interactions [33] and Goedecker–Teter–Hutter pseudopotentials [34, 35] with the double-ζ Gaussian basis sets [36]. Energy cutoffs were 400 Ry in molecular dynamics simulations and 600 Ry in static calculations. Temperature (default value 600 K) was controlled through "canonical-sampling-through-velocity-rescaling" thermostat [37]. Constant stress and constant pressure were imposed through Nose–Hoover chain barostats [38].

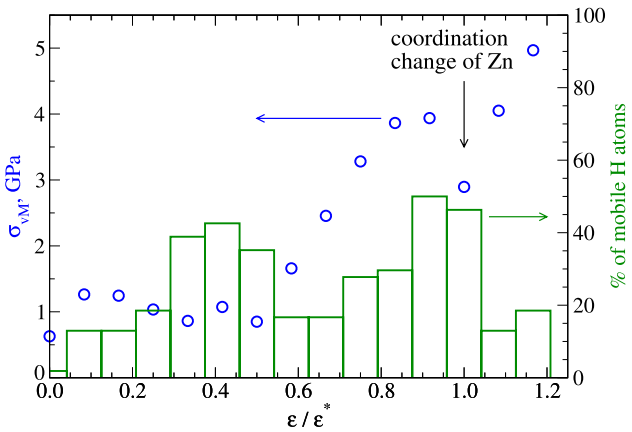

Fig. 3 Von Mises stress as a function of (compressive) strain and the lower bound for the percentage of mobile hydrogen atoms for mode (b). The strain is normalized by its value $\varepsilon^* \approx 0.24$ at which the coordination number of one zinc atom changes from 4 to 5

In *NpT*-simulations, pressure was changed in steps of 1 GPa. At each pressure, the system was given 10 ps to thermally equilibrate under isotropic volume changes, which corresponds to an effective pressure rate of 0.1 GPa/ps. In strain-controlled simulations, the strain was changed in quanta of 0.02 (with respect to the initial configuration), which was followed by equilibration periods of 6 ps leading to an effective strain rate of approximately 3.3 GHz. In minimum energy calculations, box shape and atomic coordinates were allowed to relax. Energy differences reported further below always refer to those between relaxed structures.

2.2 Initial Configuration

Starting point of our simulations are two triphosphoric acid ($P_3O_{10}H_5$) and two zinc phosphate ($Zn[PO_4H_2]_2$) molecules. The response of these molecules to isotropic stress was investigated before [16] to rationalize the stress-induced formation of anti-wear films. This is why we (rightfully) expected interesting mechanochemistry to happen. The molecular Lewis structures are shown in Fig. 1a and b, respectively. Initially, the four molecules are placed in a cubic simulation cell with a volume of $V = (3\,\mathrm{nm})^3$, and then compressed to $V = (1.2\,\mathrm{nm})^3$ within 50 ps at temperature of $T = 600$ K. Next, an external pressure $p = 0.5$ GPa was applied and the system equilibrated for 20 ps at the same temperature. During this time, all covalent, ionic, and mixed bonds remain intact. However, due to the rotation of terminal groups and other molecular rearrangements, the hydrogen-bond network changes over a-few-picoseconds timescales. Although the simulation cell is kept cubic at all times and the final, dense configurations are space-filling, see Fig. 1c′, which shows one of three starting structures. It turns out that it is possible to represent the resulting structures as a single linear molecule with side groups, which is done in Fig. 1c. By virtue of periodic boundary conditions, the chain is formally infinitely long, though we would not expect long chains to be periodic if larger system sizes could be afforded computationally.

2.3 Deformations of the Unit Cell

After thermal equilibration, the system was compressed in three different modes: (a) isotropic compression, (b) area-conserving, uniaxial compression, and (c) volume-conserving uniaxial compression. During (b), the area normal to the direction of compression remained fixed, while in (c) it was scaled such that the volume of the simulation cell was constant. Typical deformation modes in a high-pressure diamond-anvil-cell experiments are close to mode (a). Ball milling and tribological contacts would frequently lie somewhere between (b) and (c) whenever normal contact forces clearly exceed lateral forces, a situation which we refer to as "implicit or no explicit shear." The precise location of such a stress state would depend on the Poisson's ratio ν of the compressed material, e.g., it would be close to compression mode (b) for $\nu = 0$ and to mode (c) for $\nu = 1/2$. The final configuration of the simulation at fixed strain (or pressure), in which the coordination of one zinc atom changed from four to five, was used as a starting configuration for a subsequent decompression. During decompression, all degrees of freedom were allowed to fully relax to zero stress and minimum energy, that is, every atomic coordinate as well as the 6 degrees of freedom specifying the simulation cell, which are three lengths and three angles. Each deformation mode was studied with two independent starting configurations. For the non-isotropic modes (b) and (c), structures were compressed along x, y, and z-axes, which results in six independent simulations total. For completeness sake, we wish to mention that further substantial chemical modifications were only observed when stresses were so high that a sixfold coordination of Zn atoms was produced, which happened well above 10 GPa during isotropic compression, consistent with previous works [16, 39].

3 Results

We applied compressive deformations to samples, which were prepared as described in Sect. 2.2 and then pressurized and decompressed as described in Sect. 2.3. The Lewis structures of randomly chosen, decompressed systems—selected from typically nine configurations starting from the same initial structure but using different compression direction or random seeds for the thermostat—are shown in the top row of Fig. 2a–c reflecting, in this order, deformation modes (a)–(c), while the three-dimensional structures are shown in the bottom row. Lewis structures were drawn by first connecting hydrogen to oxygen atoms and next oxygen to phosphor atoms so that the octet rule was satisfied. In a few structures, not any of those selected for Fig. 2, some ambiguity remained on where to place double bonds between P and O. This ambiguity was lifted by selecting those Lewis structures that produced the smallest number of formal charges. The same principle was applied to classifying Zn–O bonds as ionic or covalent.

One compression/decompression cycle usually led to similarly looking products, although some runs produced protonated phosphoric acid molecules, while others didn't. Yet, reaction energies and elastic properties differed little from one simulation to the next for a given compression mode. In contrast, different deformation modes resulted in clearly distinct products and properties.

Some general observations, valid for each of the investigated compression/decompression modes, can be made.

One zinc atom remains four coordinated with oxygen while the other forms an additional bond with another oxygen atom. Distorted tetrahedral and distorted square pyramidal molecular geometry are adopted around four and five-coordinated zinc atoms, respectively. In each structure, at least one, usually two net proton transfers between phosphate groups occurred resulting in ionic or zwitterionic products after decompression leading to the same number of formal charges. However, already during compression, a significant fraction of hydrogen atoms changed the oxygen atom that they had been bonded to, even if the affected phosphate groups remained formally unaltered over the entire cycle.

The percentage of such "mobile" hydrogen atoms, or, rather, mobile protons, occurring on average during the 6 ps time scale between the initial and final structure of a simulation at fixed strain tensor is reported in Fig. 3 for mode (b). In the investigated strain range, three domains are observed: An initial increase of mobile protons up to a (compressive) strain of 0.1, i.e., at $\epsilon/\epsilon^* \approx 0.4$, followed by a first sudden drop. In this strain range, the von Mises stress, σ_{vM}, which is a measure of stress anisotropy or shear stress, is relatively constant. A second domain of increasing proton mobility follows, where this time, σ_{vM} increases with increasing compression. The second domain also terminates with a drop in the number of mobile protons and a quasi-discontinuous decrease of σ_{vM}. At the high-strain end of this second domain, the coordination number of one zinc atom increases from 4 to 5. Immediately after the final coordination on the zinc cation was acquired, only a few protons remained mobile in the compressed state, in particular those associated with charged groups. Even those protons became immobile once the systems had been decompressed, i.e., relaxed to the next available, zero-stress energy minimum, and then re-equilibrated at 450 K.

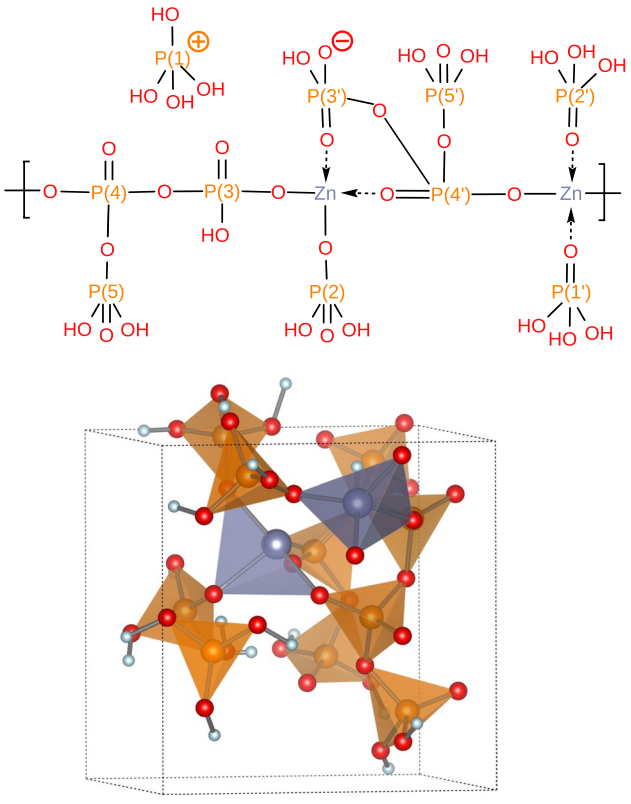

Fig. 4 Lewis and three-dimensional structure of the system after heating it to 1500 K and cooling it back down to room temperature. Color coding and other details as in Fig. 2 (Color figure online)

To elucidate, whether the large number of mobile protons was singular events allowing the terminal phosphate groups to acquire a new mechanically stable position or instead indicative of a large proton mobility at that given state of being strained, selected configurations were allowed to further equilibrate at that given state point. The numbers reduced typically reduced to 85% of the previous value. We thus conclude that the number of mobile protons is sensitive to the strain.

The just-reported characteristics were similar for all three compression modes. The points of the second transition, at which the coordination number change of zinc occurred, were, on average, $(p, \sigma_{vM}) =$ (a) (4.0, 1.2), (b) (3.1, 3.9) and (c) (1.2, 2.1), each time in units of GPa. Moreover, in modes (a) and (c) similar trends are found for the proton mobility and the von Mises stress as those reported in Fig. 3 for mode (b). However, the relative effects for the von Mises stress are smaller for the isotropic compression than for mode (b) and (c) and would vanish altogether for larger samples or if the stress tensors of different random realizations were averaged before evaluating σ_{vM}.

In addition to different stress-tensor invariants at which the coordination of Zn changes, different deformation modes lead to different characteristics in the final structures. The degree of structural rearrangement increases, not surprisingly, with increasing deformation anisotropy, i.e., with increasing (implicit) shear. Most notably, mode (c) leads to the transfer of a Zn atom from the molecular backbone to a side group. Moreover, only one Zn–O bond breaks in modes (a) and (b), while two break in mode (c), which can be deduced from Fig. 2, in which the Zn atom shown on the right-hand side is always the same Zn atom as that shown to the right in the starting structure. The involved oxygen atoms are (a) the one bridging the right Zn and P(4′) in the original Lewis structure, (b) the left Zn and P(4), and (c) the left Zn and P(4′) as well as the right Zn and P(1′). As final detail, we wish to add that in mode (a), the P(4′) unit moves from the backbone to the side chain, while P(2) is first on the side chain and moves into the backbone, whereby the number of backbone atoms is reduced from eight to six. In mode (b), a similar change occurred, however, this time involving P(4) and P(2′). We note that no P–O bond was broken in any

compression run; however, their bond order was occasionally subject to change.

The just-reported statistics are produced irrespective of the choice of the compression axis, although the precise nature of the products differed each time and it appeared to be random which of the two zinc atoms became pentacoordinate. A similar stress-induced coordination change in zinc *ortho*-phosphate [α-$Zn_3(PO_4)_2$] was observed to occur near a hydrostatic pressure of 9 GPa in a combined experimental, theoretical study and attributed to the ability of Zn to grasp on to additional oxygen atoms by hybridizing a *d* orbital with a *p* orbital of a bridging oxygen into a σ bond [40]. The insensitivity of our main results (number of produced ions, energy of reaction, final bulk modulus, number of mobile atoms during high compression) on the direction of compression in a sample as small as ours could result from the relatively high symmetry of the tetrahedral bonding on zinc and phosphorous atoms and the relatively large number of terminating OH groups making them originally point in quasi-random directions.

A few additional details are worth discussing. All deformation-induced reactions generally lead to the formation of zwitterions, although free ions—completely detached from the backbone—are also produced occasionally in the form of protonated phosphoric acid molecules, similar to the structures discussed further below for the thermally treated samples. Although *isolated*, singly positively charged $P(OH)_4$ molecules would probably not form in gas-phase or solution chemistry, an isolated molecule remained stable over more than 10 ps at temperatures of 900 K and 1500 K in a DFT simulation. In contrast, we found an *isolated*, neutral $P(OH)_4$ molecule to spontaneously decompose at room temperature into a hydrogen radical and a phosphoric acid molecule.

To compare stress with temperature-induced reactions, we first heated the system to 1000 K, while avoiding evaporation by setting the pressure to $p = 0.5$ GPa. This value of temperature is already beyond the estimates, which are often believed to occur at small scales in tribological contacts as advocated by the hot-spot model [41]. Temperature was then brought back down in discrete steps of 300 K, allowing the system to relax for 5 ps at each step, which was long enough for the enthalpy to reach a regime where signs of relaxation were hidden in thermal noise. Although roughly half of all protons in the system became mobile at 1000 K, the system reverted back to the original Lewis structure after cooling. True chemical changes and the formation of ions required the temperature to be set up as high as 1500 K within the 10 ps time span of a simulation. In the 1500 K annealing run, about 70% of protons changed the oxygen they were originally bonded to, and a protonated phosphoric acid molecule formed together with a negatively charged backbone molecule. After cooling, the charges remained on the entities on which they were generated. The final space-filling structure and its Lewis structure are shown in Fig. 4. During cooling, roughly 50% of the protons remained mobile, which is a similar ratio as during heating before ions were formed. When going down further to 500 K, only 10–15% hydrogens remained mobile. We note in passing that going up to 5000 K leads to the formation of three water molecules, which, however, required the breaking of P–O bonds. It is outside the scope of this work to assess if the latter reactions would occur on experimental time scales at lower temperature.

The thermal cycles were endothermic with an energy of reaction of $\Delta E = 0.138$ eV for $T = 1500$ K and $\Delta E = 0.507$ eV for $T = 5000$ K per Zn atom, while all stress cycles were exothermic with ΔE ranging from -0.077 eV for mode (c) to -0.195 eV for mode (a) compression. Given our results, the occasionally made assumption that mechanochemistry results predominantly from local heating, as advocated in the hot-spot model [41], seems unlikely for our system of interest. In addition, we are somewhat skeptical of typical flash-temperature estimates as they tend to assign the dissipated energy to a small interfacial zone, although important dissipative processes contributing substantially to friction, such as viscoelastic or plastic deformation, also take place far away from it.

4 Potential Relevance to Triboelectricity

We believe our results on stress-induced ionization to matter in the context of triboelectricity. Although the required *local* stresses of order 1 GPa may appear large from a continuum perspective, linear-elasticity theory predicts them to be of order root-mean-square height gradient times the smaller Young's modulus of the contacting materials [42]. They can exceed the macroscopic hardness, because plasticity-inducing defects are not energetically favorable at small scales and/or because of inertial confinement in a short-lasting asperity collision. Thus, even contacts formed by amber and keratin (wool, fur, epidermis of skin, etc.), which both have relatively large Young's modulus and form the basis of the classical amber against wool or cat-fur triboelectricity couple [7], must be expected to reach local values exceeding 1 GPa.

Nernst [43] speculated a long time ago that tribo-charging between insulators is due to ion transfer. He proposed various equations describing how ions account for contact-induced charging in response to gradients or interfacial differences in chemical composition, ion concentration, temperature, pressure, and the like. A prominent example of the processes that Nernst thus might have foreseen is the tribo-charging of falling Graupel sliding past small ice crystals rising in a thundercloud. Central parameters in

Nernst's discussion are ionic mobilities and number densities, which are utterly sensitive to stress in our model phosphate at typical contact stresses. It may appear daring to discuss triboelectricity w.r.t. our phosphates, in light of its (current) absence in popular triboelectric series [44, 45], in which material A is placed above material B if A acquires a positive charge through rubbing against B. Nonetheless, dry phosphate ores seem prone to triboelectric charging, because they can be beneficiated with triboelectric belt separators [46, 47].

A careful review of the literature [48] should prevent one from making strong claims of one mechanism, let alone one material property, to be the sole key to understand tribo-induced charging between insulators, even if it is enticing and in each case justifiable to correlate the (fuzzy) triboelectrical series according to the materials' dielectric constant [49], pK_a [50], Seeman [51], or flexoelectric coefficients [52]. As is the case for the origin of friction, where strikingly different microscopic mechanisms can lead to identical macroscopic friction laws [53], triboelectricity being one of them [54], the question to be answered is not what single mechanism explains everything but which mechanism dominates under what circumstances and how can we figure out, theoretically or experimentally, which one it is? In fact, the existence of a *cyclic* triboelectric series [8], where material A is more tribopositive than B than C than A—somewhat reminiscent of the stairs in the famous lithography *Ascending and Descending* by the Dutch artist Maurits Cornelis Escher (1960)—appears to indicate that there is not a single dominant tribo-charging mechanism for the AB, BC, and CA interfaces. Likewise, the reversal of charging direction with increasing rubbing time [49, 55] can be seen as an indicator for the existence of competing tribo-charge carriers potentially having different response times.

While regular ion-transfer charging can already be at the root of various triboelectric observations, such as the charging between dielectrics of identical chemistry but different size [56, 57] or mosaics of positive and negative domains [58], additional phenomena might have their root in stress-enhanced ionization. This concerns in particular how strain alters the position of some materials in the triboelectric series [59, 60] and the correlation of the latter with their pK_a [50], which appears natural, since a material with a large propensity to donate protons to an electrolyte will also release them under stress. Such an effect could even radically change the positioning of a material in a triboelectric series, e.g., when it has stress-releasable protons in addition to nucleobase moieties. In well-defined, single-asperity contacts, free ions would only be expected to occur above a certain threshold force and explicit stress would enhance but not be required for tribo-charges to be generated. In randomly rough surfaces, the repositioning of a material in a triboelectric series due to increased surface roughness [61] could simply result from an increased rms-height gradients and thus increased contact stresses. We certainly do not mean to imply that the observation of every discussed phenomenon automatically implies stress-induced ionization to be responsible for it. However, given the ease with which ions can be apparently created under stress, our bias has certainly shifted toward the "ion-transfer school," despite of having made large efforts in the past toward the design of empirical electron-transfer potentials describing tribo-charging between dielectrics [62].

5 Conclusions

To summarize, our simulations on phosphates revealed a significant stress-induced (zwitter) ionization at stresses that appear unavoidable in tribological contacts, where similar molecules are used as anti-wear and anti-oxidant additives. The final molecular structures turned out to depend sensitively on the precise shape of the stress tensor during compression and differed again from those obtained through thermal activation at moderate hydrostatic stresses. This observation provides theoretical support but also refinement of the experimentally acquired picture that tribo-charging can originate from the creation of radicals through mechanochemistry [63, 64]. The large number of ions produced in our simulations—protons were mobilized long before the quasi-discontinuous changes in enthalpy occurred, e.g., at $p \approx 0.6$ GPa and $\sigma_{vM} = 2$ GPa—should certainly suffice to create a net imbalance of one elementary charge per 100,000 surface atoms, which is the value needed to yield tribo-voltages of several thousand volts on insulators [60]. The targeted exploration of the stress-induced ionization via simulations might benefit the search for triboelectrically active materials. Stress-released ions could lead to large tribo-voltages on a first stroke and thus be desired. However, they could also be detrimental should it be difficult to chemically rejuvenate the material after exploitation of the tribo-voltage. In any event, it seems clear that gas-phase chemical considerations for the functionality of materials in contact situations might have to be augmented with analysis similar to ours, in order to ascertain if or how a certain substance or material fulfills its requirements for the expected contact conditions.

Funding Open Access funding enabled and organized by Projekt DEAL. Support by the Deutsche Forschungsgemeinschaft (DFG) through Grant MU 1694/5-2 is acknowledged.

Declarations

Conflict of interest The authors have no relevant financial or non-financial interests to disclose.

References

1. Beyer, M.K., Clausen-Schaumann, H.: Mechanochemistry: the mechanical activation of covalent bonds. Chem. Rev. **105**(8), 2921 (2005). https://doi.org/10.1021/cr030697h
2. James, S.L., Adams, C.J., Bolm, C., Braga, D., Collier, P., Friščić, T., Grepioni, F., Harris, K.D.M., Hyett, G., Jones, W., Krebs, A., Mack, J., Maini, L., Orpen, A.G., Parkin, I.P., Shearouse, W.C., Steed, J.W., Waddell, D.C.: Mechanochemistry: opportunities for new and cleaner synthesis. Chem. Soc. Rev. **41**(1), 413 (2012). https://doi.org/10.1039/c1cs15171a
3. O'Neill, R.T., Boulatov, R.: The many flavours of mechanochemistry and its plausible conceptual underpinnings. Nat. Rev. Chem. **5**(3), 148 (2021). https://doi.org/10.1038/s41570-020-00249-y
4. Akbulatov, S., Boulatov, R.: Experimental polymer mechanochemistry and its interpretational frameworks. ChemPhysChem **18**(11), 1422 (2017). https://doi.org/10.1002/cphc.201601354
5. Michalchuk, A.A.L., Boldyreva, E.V., Belenguer, A.M., Emmerling, F., Boldyrev, V.V.: Tribochemistry, mechanical alloying, mechanochemistry: what is in a name? Front. Chem. (2021). https://doi.org/10.3389/fchem.2021.685789
6. Kaupp, G.: Mechanochemistry: the varied applications of mechanical bond-breaking. CrystEngComm **11**(3), 388 (2009). https://doi.org/10.1039/b810822f
7. Iversen, P., Lacks, D.J.: A life of its own: the tenuous connection between Thales of Miletus and the study of electrostatic charging. J. Electrost. **70**(3), 309 (2012). https://doi.org/10.1016/j.elstat.2012.03.002
8. McCarty, L., Whitesides, G.: Electrostatic charging due to separation of ions at interfaces: contact electrification of ionic electrets. Angew. Chem. Int. Ed. **47**(12), 2188 (2008). https://doi.org/10.1002/anie.200701812
9. Badro, J., Teter, D.M., Downs, R.T., Gillet, P., Hemley, R.J., Barrat, J.L.: Theoretical study of a five-coordinated silica polymorph. Phys. Rev. B **56**(10), 5797 (1997). https://doi.org/10.1103/physrevb.56.5797
10. Zhang, R., Cai, W., Bi, T., Zarifi, N., Terpstra, T., Zhang, C., Verdeny, Z.V., Zurek, E., Deemyad, S.: Effects of nonhydrostatic stress on structural and optoelectronic properties of methylammonium lead bromide perovskite. J. Phys. Chem. Lett. **8**(15), 3457 (2017). https://doi.org/10.1021/acs.jpclett.7b01367
11. Gao, Y., Ma, Y., An, Q., Levitas, V., Zhang, Y., Feng, B., Chaudhuri, J., Goddard, W.A.: Shear driven formation of nano-diamonds at sub-gigapascals and 300 K. Carbon **146**, 364 (2019). https://doi.org/10.1016/j.carbon.2019.02.012
12. Zhang, J., Ewen, J.P., Spikes, H.A.: Substituent effects on the mechanochemical response of zinc dialkyldithiophosphate. Mol. Syst. Des. Eng. (2022). https://doi.org/10.1039/d2me00049k
13. Nicholls, M.A., Do, T., Norton, P.R., Kasrai, M., Bancroft, G.: Review of the lubrication of metallic surfaces by zinc dialkyldithiophosphates. Tribol. Int. **38**(1), 15 (2005). https://doi.org/10.1016/j.triboint.2004.05.009
14. Zhang, J., Spikes, H.: On the mechanism of ZDDP antiwear film formation. Tribol. Lett. (2016). https://doi.org/10.1007/s11249-016-0706-7
15. Nicholls, M.A., Do, T., Norton, P.R., Bancroft, G.M., Kasrai, M., Capehart, T.W., Cheng, Y.T., Perry, T.: Tribol. Lett. **15**(3), 241 (2003). https://doi.org/10.1023/a:1024813203442
16. Mosey, N.J., Müser, M.H., Woo, T.K.: Molecular mechanisms for the functionality of lubricant additives. Science **307**(5715), 1612 (2005). https://doi.org/10.1126/science.1107895
17. Shakhvorostov, D., Nicholls, M.A., Norton, P.R., Müser, M.H.: Mechanical properties of zinc and calcium phosphates. Eur. Phys. J. B **76**(3), 347 (2010). https://doi.org/10.1140/epjb/e2010-00193-3
18. Gosvami, N.N., Bares, J.A., Mangolini, F., Konicek, A.R., Yablon, D.G., Carpick, R.W.: Mechanisms of antiwear tribofilm growth revealed in situ by single-asperity sliding contacts. Science **348**(6230), 102 (2015). https://doi.org/10.1126/science.1258788
19. Naveed, A., Yang, H., Yang, J., Nuli, Y., Wang, J.: Highly reversible and rechargeable safe Zn batteries based on a triethyl phosphate electrolyte. Angew. Chem. Int. Ed. **58**(9), 2760 (2019). https://doi.org/10.1002/anie.201813223
20. Vijayakumar, M., Bain, A.D., Goward, G.R.: Investigations of proton conduction in the monoclinic phase of RbH_2PO_4 using multinuclear solid-state NMR. J. Phys. Chem. C **113**(41), 17950 (2009). https://doi.org/10.1021/jp903408v
21. Inukai, M., Horike, S., Itakura, T., Shinozaki, R., Ogiwara, N., Umeyama, D., Nagarkar, S., Nishiyama, Y., Malon, M., Hayashi, A., Ohhara, T., Kiyanagi, R., Kitagawa, S.: Encapsulating mobile proton carriers into structural defects in coordination polymer crystals: high anhydrous proton conduction and fuel cell application. J. Am. Chem. Soc. **138**(27), 8505 (2016). https://doi.org/10.1021/jacs.6b03625
22. O'Keeffe, M., Perrino, C.: Proton conductivity in pure and doped KH_2PO_4. J. Phys. Chem. Solids **28**(2), 211 (1967). https://doi.org/10.1016/0022-3697(67)90110-2
23. Boysenand, D.A., Haile, S.M., Liu, H., Secco, R.A.: High-temperature behavior of CsH_2PO_4 under both ambient and high pressure conditions. Chem. Mater. **15**(3), 727 (2003). https://doi.org/10.1021/cm020138b
24. Matsuda, A., Kikuchi, T., Katagiri, K., Muto, H., Sakai, M.: Structure and proton conductivity of mechanochemically treated $50CsHSO_4.50CsH_2PO_4$. Solid State Ion. **177**(26–32), 2421 (2006). https://doi.org/10.1016/j.ssi.2006.03.053
25. Paschos, O., Kunze, J., Stimming, U., Maglia, F.: A review on phosphate based, solid state, protonic conductors for intermediate temperature fuel cells. J. Phys. Condens. Matter **23**(23), 234110 (2011). https://doi.org/10.1088/0953-8984/23/23/234110
26. Mosey, N.J., Woo, T.K., Müser, M.H.: Phys. Rev. B (2005). https://doi.org/10.1103/physrevb.72.054124
27. Schmidt, C., Pommerenke, H., Dürr, F., Nebe, B.: Energy dissipation via quantum chemical hysteresis during high-pressure compression: a first-principles molecular dynamics study of phosphates. J. Rychly, J. Biol. Chem. **273**(9), 5081 (1998). https://doi.org/10.1074/jbc.273.9.5081
28. Sukhomlinov, S.V., Müser, M.H.: Stress anisotropy severely affects zinc phosphate network formation. Tribol. Lett. **69**, 3 (2021). https://doi.org/10.1007/s11249-021-01462-6
29. Hohenberg, P., Kohn, W.: Inhomogeneous electron gas. Phys. Rev. **136**(3B), B864 (1964). https://doi.org/10.1103/physrev.136.b864

30. Kohn, W., Sham, L.J.: Self-consistent equations including exchange and correlation effects. Phys. Rev. **140**(4A), A1133 (1965). https://doi.org/10.1103/physrev.140.a1133
31. Hutter, J., Iannuzzi, M., Schiffmann, F., de Vondele, J.V.: cp2k:atomistic simulations of condensed matter systems. Wiley Interdiscip. Rev. Comput. Mol. Sci **4**(1), 15 (2013). https://doi.org/10.1002/wcms.1159
32. Perdew, J.P., Ernzerhof, M., Burke, K.: Rationale for mixing exact exchange with density functional approximations. J. Chem. Phys. **105**(22), 9982 (1996). https://doi.org/10.1063/1.472933
33. Grimme, S., Antony, J., Ehrlich, S., Krieg, H.: A consistent and accurate ab initio parametrization of density functional dispersion correction (DFT-D) for the 94 elements H–Pu. J. Chem. Phys. **132**(15), 154104 (2010). https://doi.org/10.1063/1.3382344
34. Goedecker, S., Teter, M., Hutter, J.: Separable dual-space Gaussian pseudopotentials. Phys. Rev. B **54**(3), 1703 (1996). https://doi.org/10.1103/physrevb.54.1703
35. Hartwigsen, C., Goedecker, S., Hutter, J.: Relativistic separable dual-space Gaussian pseudopotentials from H to Rn. Phys. Rev. B **58**(7), 3641 (1998). https://doi.org/10.1103/physrevb.58.3641
36. de Vondele, J.V., Hutter, J.: Gaussian basis sets for accurate calculations on molecular systems in gas and condensed phases. J. Chem. Phys. **127**(11), 114105 (2007). https://doi.org/10.1063/1.2770708
37. Bussi, G., Donadio, D., Parrinello, M.: Canonical sampling through velocity rescaling. J. Chem. Phys. **126**(1), 014101 (2007). https://doi.org/10.1063/1.2408420
38. Martyna, G.J., Klein, M.L., Tuckerman, M.: Nosé–Hoover chains: the canonical ensemble via continuous dynamics. J. Chem. Phys. **97**(4), 2635 (1992). https://doi.org/10.1063/1.463940
39. Shakhvorostov, D., Müser, M.H., Mosey, N.J., Song, Y., Norton, P.R.: Correlating cation coordination, stiffness, phase transition pressures, and smart materials behavior in metal phosphates. Phys. Rev. B **79**(9), 094107 (2009). https://doi.org/10.1103/PhysRevB.79.094107
40. Shakhvorostov, D., Müser, M.H., Mosey, N.J., Munoz-Paniagua, D.J., Pereira, G., Song, Y., Kasrai, M., Norton, P.R.: J. Chem. Phys. **128**(7), 074706 (2008). https://doi.org/10.1063/1.2837809
41. Tricker, A.W., Samaras, G., Hebisch, K.L., Realff, M.J., Sievers, C.: On the pressure-induced loss of crystallinity in *ortho*phosphates of zinc and calcium. Chem. Eng. J. **382**, 122954 (2020). https://doi.org/10.1016/j.cej.2019.122954
42. Persson, B.N.J.: Theory of rubber friction and contact mechanics. J. Chem. Phys. **115**(8), 3840 (2001). https://doi.org/10.1063/1.1388626
43. Nernst, W.: Ueber Berührungselectricität. Ann. Phys. (Berl.) **294**(8), i (1896). https://doi.org/10.1002/andp.18962940815
44. Lacks, D.J.: The unpredictability of electrostatic charging. J. Electrost. **51**(28), 6822 (2012). https://doi.org/10.1002/anie.201202896
45. Zou, H., Zhang, Y., Guo, L., Wang, P., He, X., Dai, G., Zheng, H., Chen, C., Wang, A.C., Xu, C., Wang, Z.L.: Quantifying the triboelectric series. Nat. Commun. **10**(1), 1427 (2019). https://doi.org/10.1038/s41467-019-09461-x
46. Tao, D., Al-Hwaitti, M.: Beneficiation study of Eshidiya phosphorites using a rotary triboelectrostatic separator. Min. Sci. Technol. (China) **20**(3), 357 (2010). https://doi.org/10.1016/s1674-5264(09)60208-8
47. Bittner, J., Hrach, F., Gasiorowski, S., Canellopoulus, L., Guicherd, H.: Triboelectric belt separator for beneficiation of fine minerals. Procedia Eng. **83**, 122 (2014). https://doi.org/10.1016/j.proeng.2014.09.021
48. Lacks, D.J., Shinbrot, T.: Long-standing and unresolved issues in triboelectric charging. Nat. Rev. Chem. **3**(8), 465 (2019). https://doi.org/10.1038/s41570-019-0115-1
49. Coehn, A.: Ueber ein Gesetz der Electricitätserregung. Ann. Phys. **64**(300), 217 (1898). https://doi.org/10.1002/andp.18983000203
50. Diaz, A., Felix-Navarro, R.: A semi-quantitative tribo-electric series for polymeric materials: the influence of chemical structure and properties. J. Electrost. **62**(4), 277 (2004). https://doi.org/10.1016/j.elstat.2004.05.005
51. Shin, E.C., Ko, J.H., Lyeo, H.K., Kim, Y.H.: Derivation of a governing rule in triboelectric charging and series from thermoelectricity. Phys. Rev. Res. **4**(2), 023131 (2022). https://doi.org/10.1103/physrevresearch.4.023131
52. Mizzi, C., Lin, A., Marks, L.: Does flexoelectricity drive triboelectricity? Phys. Rev. Lett. **123**(11), 116103 (2019). https://doi.org/10.1103/physrevlett.123.116103
53. Müser, M.H., Urbakh, M., Robbins, M.O.: Statistical mechanics of static and low-velocity kinetic friction. In: Advances in Chemical Physics, pp. 187–272. Wiley (2003). https://doi.org/10.1002/0471428019.ch5
54. Burgo, T.A.L., Silva, C.A., Balestrin, L.B.S., Galembeck, F.: Friction coefficient dependence on electrostatic tribocharging. Sci. Rep. (2013). https://doi.org/10.1038/srep02384
55. Baytekin, H.T., Baytekin, B., Incorvati, J.T., Grzybowski, B.A.: Material transfer and polarity reversal in contact charging. Angew. Chem. Int. Ed. **124**(20), 4927 (2012). https://doi.org/10.1002/ange.201200057
56. Zhao, H., Castle, G., Inculet, I.: The measurement of bipolar charge in polydisperse powders using a vertical array of Faraday pail sensors. J. Electrost. **55**(3–4), 261 (2002). https://doi.org/10.1016/s0304-3886(01)00209-1
57. Bilici, M.A., Toth, J.R., Sankaran, R.M., Lacks, D.J.: Particle size effects in particle–particle triboelectric charging studied with an integrated fluidized bed and electrostatic separator system. Rev. Sci. Instrum. **85**(10), 103903 (2014). https://doi.org/10.1063/1.4897182
58. Baytekin, H.T., Patashinski, A.Z., Branicki, M., Baytekin, B., Soh, S., Grzybowski, B.A.: The mosaic of surface charge in contact electrification. Science **333**(6040), 308 (2011). https://doi.org/10.1126/science.1201512
59. Shaw, P.E.: Experiments on tribo-electricity. I.—The tribo-electric series. Proc. R. Soc. Lond. A **94**(656), 16 (1917). https://doi.org/10.1098/rspa.1917.0046
60. Sow, M., Widenor, R., Kumar, A., Lee, S.W., Lacks, D.J., Sankaran, R.M.: Strain-induced reversal of charge transfer in contact electrification. Angew. Chem. Int. Ed. **51**(11), 2695 (2012). https://doi.org/10.1002/anie.201107256
61. Wang, A.E., Greber, I., Angus, J.C.: Contact charge transfer between inorganic dielectric solids of different surface roughness. J. Electrost. **101**, 103359 (2019). https://doi.org/10.1016/j.elstat.2019.103359
62. Dapp, W.B., Müser, M.H.: Towards time-dependent, non-equilibrium charge-transfer force fields. Eur. Phys. J. B (2013). https://doi.org/10.1140/epjb/e2013-40047-x
63. Henniker, J.: Triboelectricity in polymers. Nature **196**(4853), 474 (1962). https://doi.org/10.1038/196474a0
64. Baytekin, B., Baytekin, H.T., Grzybowski, B.A.: What really drives chemical reactions on contact charged surfaces? J. Am. Chem. Soc. **134**(17), 7223 (2012). https://doi.org/10.1021/ja300925h